BJRS
BRAZILIAN JOURNAL OF RADIATION SCIENCES

doi.org/10.15392/2319-0612.2025.2958
Braz. J. Radiat. Sci., Rio de Janeiro
2025, 13(4) | 01-26 | e2958
Editor: Prof. Dr. Bernardo Maranhão Dantas
Editor: Prof. Dr. Alfredo Lopes Ferreira Filho
Submitted: 2025-05-31
Accepted: 2025-09-11

Monte Carlo simulation of a 6 MV Varian Trilogy clinical linear accelerator using Geant4 for small-field dosimetry analysis

Ribeiro[a], A. L. C.; De Oliveira[b], A. C. H; Da Silva[c], L. P.; De Paiva[a*], E.

[a]Instituto de Radioproteção e Dosimetria, 22783-127, Rio de Janeiro, Brazil.
[b]Faculdade Nova Esperança, 58067-695, João Pessoa, Brazil
[c]Instituto Nacional de Câncer, 20230-130, Rio de Janeiro, Brazil

*Correspondence: eduardo.paiva@ird.gov.br

Abstract: In recent decades, radiotherapy has advanced significantly due to the emergence of advanced clinical linear accelerators, enabling safer and faster treatments with reduced side effects. In this study, we present a Monte Carlo simulation of a 6 MV Varian Trilogy clinical linear accelerator using the Geant4 toolkit to analyze dosimetric parameters, with a focus on small photon fields. The simulation models phase-space files generated at key beam-modification stages. Validation was performed by comparing simulated depth dose curves (PDD) and dose profiles with experimental measurements for the 6 MV photon beam, employing the gamma index (3%/3 mm criteria) to quantify the degree of agreement in the PDDs. The results agreed within a 2% difference, with over 95% of points passing the gamma analysis for a 10 x 10 cm² field. The developed framework allows for the calculation of correction factors for small-field dosimetry, addressing challenges such as lateral electronic disequilibrium in high-energy 6 MV beams, and comparing them with established values in the literature. These capabilities are particularly important for measurements of small fields used in advanced radiotherapy techniques, including Stereotactic Radiosurgery (SRS) and Stereotactic Body Radiotherapy (SBRT), where high precision in dose deposition is essential. Overall, this work establishes a robust and flexible Geant4-based platform for simulating clinical linear accelerators, contributing to the development of more accurate dosimetric protocols for high-energy photon therapy in small fields. Preliminary observations suggest notable output factor discrepancies in small photon fields (<3x3 cm²), indicating the potential need for detector-specific correction factors. Ongoing analysis aims to confirm these trends.

Keywords: Monte Carlo simulation, Geant4, Varian Trilogy, small field dosimetry, gamma index, radiotherapy.

doi.org/10.15392/2319-0612.2025.2958
Braz. J. Radiat. Sci., Rio de Janeiro
2025, 13(4) | 01-26 | e2958
Editor: Prof. Dr. Bernardo Maranhão Dantas
Editor: Prof. Dr. Alfredo Lopes Ferreira Filho
Submitted: 2025-05-31
Accepted: 2025-09-11

Simulação de Monte Carlo de um acelerador linear clínico Varian Trilogy de 6 MV usando Geant4 para análise dosimétrica em campos pequenos

Resumo: Nas últimas décadas a radioterapia se desenvolveu bastante em função do surgimento de aceleradores lineares clínicos avançados, permitindo tratamentos mais seguros e rápidos, com redução de efeitos colaterais. Neste estudo, apresentamos uma simulação de Monte Carlo de um acelerador linear clínico Varian Trilogy de 6 MV utilizando a ferramenta Geant4 para analisar parâmetros dosimétricos, com foco em campos pequenos de fótons. A simulação modela os arquivos de espaço de fase em estágios chaves de modificação do feixe. A validação foi realizada comparando curvas simuladas de dose em profundidade (PDD) e perfis de dose com medições experimentais para o feixe de fótons de 6 MV, empregando o índice gama (critérios de 3%/3 mm) para quantificar o grau de concordância nos PDD's. Os resultados concordaram em até 2% de diferença, com mais de 95% dos pontos passando na análise gama para um campo de 10 x 10 cm^2. A estrutura desenvolvida permite calcular fatores de correção para dosimetria de campos pequenos, abordando desafios como a perda de equilíbrio eletrônico lateral em feixes de alta energia de 6 MV e compará-los com os valores estabelecidos na literatura. Essas capacidades são particularmente importantes para medidas de campos pequenos utilizados em técnicas avançadas de radioterapia, incluindo Radiocirurgia (SRS) e Radioterapia Estereotáxica Corporal (SBRT), nas quais a alta precisão na deposição da dose é essencial. De modo geral, este trabalho estabelece uma plataforma robusta e flexível baseada no Geant4 para simulação de aceleradores lineares clínicos, contribuindo para o desenvolvimento de protocolos dosimétricos mais precisos na terapia com fótons de altas energias em campos pequenos. Observações preliminares sugerem discrepâncias notáveis no fator de saída em campos de fótons pequenos (<3x3cm^2), indicando a potencial necessidade de fatores de correção específicos para cada detector. Análises em andamento visam confirmar essas tendências.

Palavras-chave: simulação de Monte Carlo, Geant4, Varian Trilogy, dosimetria de campos pequenos, índice gama, radioterapia.

1. INTRODUCTION

Radiation therapy using high-energy photon beams (6-25 MV) is one of the most effective and widely employed modalities for cancer treatment, accounting for 70-80% of external beam therapies due to its deep tissue penetration and compatibility with advanced techniques [1-3]. The effectiveness of patient treatment directly benefits from advancements in dosimetric methodologies [4,5]. Over the past few decades, external photon beam radiation therapy has evolved significantly from the initial use of orthovoltage and Cobalt-60 units to the development of modern linear accelerators (Linacs). These advancements have led to various treatment techniques, including those utilizing dynamic fields, such as Stereotactic Body Radiation Therapy (SBRT), Intensity Modulated Radiation Therapy (IMRT), and Volumetric Arc Therapy (VMAT) [3,6]. These techniques often rely on small radiation fields, which introduce unique dosimetric challenges requiring specialized modeling and measurement approaches. They aim to maximize the target dose while minimizing exposure to surrounding healthy tissues. However, the increasing use of small static fields presents significant problems in dosimetry, as traditional measurement techniques struggle with high dose gradients and lack of lateral electronic equilibrium [7-13].

To address these challenges, Monte Carlo methods (MC) have become indispensable, offering high-accuracy dose calculations by simulating particle interactions at a microscopic level [14-17]. Furthermore, the simulation of linear accelerators using Monte Carlo models allows for detailed characterization of beam properties and validation of treatment planning systems. Recent studies have shown that MC simulations can enhance the reliability of dosimeter readings when appropriate correction factors are applied [9,10]. Correction factors have also been used in experimental setups to ensure high reliability in small field dosimetry. These factors exhibit specific behavior that depend on various parameters, including beam

energy, collimation method, linear accelerator geometry, and the type of dosimeter used for calibration, necessitating case-by-case determination.

In this study, we simulate the 6 MV Varian Trilogy medical Linac photon beam using the Geant4 Monte Carlo code in order to analyze physical disturbances in small photon fields and develop correction factors. Geant4 was selected as the core Monte Carlo toolkit for this study due to its versatility in handling complex geometries, customizable physics modeling, and broad validation across medical physics applications. Compared to other codes like EGSnrc and PENELOPE, Geant4 offers a more adaptable framework suitable for hybrid radiotherapy scenarios and dosimetric simulations. Additionally, we validate the simulated beam by comparing it with experimental data obtained at the Brazilian National Cancer Institute (INCa). Figure 1 shows an illustration of the Varian Trilogy Linac.

Figure 1: Varian Trilogy linear accelerator at INCa I.

Source: Varian Medical Systems website [18].

This study focuses on modeling and validating dose distributions in small radiation fields, using a 10 x 10 cm^2 reference as a foundation. While the current scope does not include fields smaller than 3 x 3 cm^2, the methodologies developed here serve as groundwork for future investigations into ultra-small fields.

2. MATERIALS AND METHODS

2.1. Geant4 Monte Carlo code

2.1.1 Application overview and toolkit features

Monte Carlo-based applications in radiotherapy simulations fall into two categories: generating phase-space (PhSp) files from a linear accelerator model, and evaluating dose distributions in computational phantoms using these PhSp files. These phantoms may incorporate anatomical or mathematical representations.

Version 11.1 of the Geant4 toolkit, developed by CERN's Geant4 Collaboration, was employed to perform Monte Carlo simulations of particle transport. For this study, we adopted the Livermore electromagnetic physics model with a 1 mm global transport cut-off, in alignment with recommended practices for small-field dosimetry [9]. This value is commonly used to ensure accurate modeling of secondary electron transport in high-gradient regions, while maintaining computational efficiency in Monte Carlo simulations. It represents the successor of the Geant series developed at CERN, and it is the first toolkit of its kind to employ object-oriented programming principles, implemented in C++.

The toolkit supports the simulation of a wide range of particles, including photons and ions, across an extensive energy spectrum - from 250 eV photons and thermal neutrons to ultra-high energies such as those encountered in cosmic ray experiments and particle collisions at the TeV scale. Monte Carlo simulations in Geant4 require the definition of core

components, including system geometry, particle definitions, and the primary particle source. These are managed through user-defined classes, which allow customization of the simulation process from particle generation to energy deposition:

i. the geometry and materials of the system (G4VUserDetectorConstruction),

ii. the particles of interest and their corresponding physical processes (G4VPhysicsConstructor),

iii. the primary particle generation (G4VUserPrimaryGeneratorAction),

iv. the main execution control (main) responsible for managing the simulation flow.

Geant4 provides a variety of fully implemented example applications, which serve as references for users aiming to develop custom simulations.

2.1.2 Simulation architecture and physics model

Geant4 organizes particle transport into a hierarchy of simulation levels: runs, events, tracks, and steps. Each level captures progressively finer details, with energy deposition occurring at the step level as particles traverse the simulation geometry:

i. Run: the highest-level simulation structure, comprising a series of identically configured events.

ii. Event: represents a single history or instance of simulation, consisting of multiple tracks.

iii. Track: defines the motion of a particle between two interactions, containing both dynamic (e.g., position, energy, direction) and static (e.g., mass, charge) properties.

iv. Step: the fundamental unit of transport, describing changes in a track between two discrete points (PreStepPoint and PostStepPoint). It is at this level that the deposited energy is calculated and updated, as the particle is transported step-by-step through the geometry.

Each simulation level is represented by a specific class: G4Run, G4Event, G4Track, and G4Step, respectively [19-21].

The interactions between particles and matter in Geant4 are governed by a range of physics models, which include processes such as Compton scattering, ionization, and bremsstrahlung. Users can select among standard electromagnetic models like Standard, Livermore, or Penelope depending on the desired balance between precision and computational cost.

For application development, it is recommended that users employ the reference physics constructors provided by Geant4. In simulations involving photons, protons, electrons, and positrons, three electromagnetic physics models are commonly used: Standard, Livermore, and Penelope. To accurately model electromagnetic interactions in the small-field dosimetry setup, the Livermore physics model was selected within Geant4. This model includes detailed atomic cross-section data sourced from EPDL97 and EEDL, enabling precise simulation of low-energy photon interactions such as photoelectric absorption, coherent scattering, and ionization - crucial processes in 6 MV beam configurations. Unlike the Standard physics list, which is optimized for higher-energy scenarios and lacks detailed low-energy atomic shell modeling, Livermore supports interactions below 1 MeV with shell-specific resolution. The Penelope model, though also suited for low-energy applications, incurs greater computational cost and complexity. Livermore provides a favorable trade-off between precision and performance while seamlessly integrating into Geant4's modular architecture and supporting fine-grained transport thresholds. These characteristics make Livermore especially suitable for small-field applications where steep dose gradients and reduced electronic equilibrium demand high-fidelity physics modeling.

Rather than using fixed energy thresholds, Geant4 applies a range-based transport cut, defining the minimum distance a secondary particle must travel to be generated. This

threshold is material-specific and translated internally to an energy value for each component. This limit is defined via the SetCut( ) method within the PhysicsList class and is internally converted to energy for each material in the simulation. For this study, a LT of 1 mm was employed as the standard.

2.1.3 Scoring systems and visualization

To facilitate data acquisition during simulations, Geant4 provides multiple tools, including sensitive detectors, scoring volumes, and user-defined actions. These features enable the tracking of key quantities such as deposited energy and particle flux at different stages of the simulation:

a) the implementation of a sensitive detector, capable of recording hits (signals) within a virtual device;

b) the definition of a scoring volume, which accumulates specific quantities such as deposited energy, particle flux, or number of interactions;

c) the use of user actions, which are custom classes defined by the user to extract information at various stages of the simulation—namely, at the run (G4UserRunAction), event (G4UserEventAction), track (G4UserTrackingAction), and step (G4UserSteppingAction) levels.

Visualization in Geant4 is supported through integration with external graphics libraries such as OpenGL and VRML. Additionally, a Qt-based graphical interface enhances user interaction, allowing inspection and control of the simulation environment. Additionally, the toolkit features a graphical user interface (GUI) built on Qt (G4UIQt), which enhances the visual inspection of simulation setups and facilitates simulation control [19-21].

2.2. Linear accelerator simulation

2.2.1 General overview

Following configuration of the simulation environment, the Linac head was modeled using a custom Geant4 implementation called qLinacs. The structure was based on an existing geometry tailored to represent the 6 MV Varian Trilogy system, incorporating high-definition MLC data provided by the manufacturer. A preexisting model from the Geant4 library was adapted to simulate a 6 MV Varian Trilogy Linac (Varian Medical Systems, USA) with a Varian Millennium high-definition MLC (HDMLC, speed of 3.5 cm/s, 40 cm x 40 cm maximum field size, 60 pairs of leaves), based on data provided by Varian [21]. The modeling data are applicable to Clinac IX, DX, C/D, EX, cX, Trilogy, and Novalis TX models, as the primary distinguishing factor among them is the primary electron beam characteristics defined by the full-width-at-half-maximum (FWHM) values of the energy and spatial distributions, as well as the mean energy. For the Monte Carlo modeling of the primary beam, the electron source was configured with a Gaussian spatial distribution and energy spread. The FWHM of the spatial distribution was set to 1.5 mm, and the energy distribution had a mean energy of 6.2 MeV, corresponding to the manufacturer's nominal 6 MV beam specifications. The particle transport cut (range cut, or LT) can be set individually for each Linac component, and the user may select from among the available Geant4 physics models.

2.2.2 Component Modeling

The Monte Carlo modeling of the Linac was composed as follows:

a) Target: two cylindrical layers of tungsten and copper, 10 mm in diameter (LT = 0.25 mm);
b) Primary collimator: a conical tungsten cylinder, 100 mm in height (LT = 50 mm);
c) The collimator aperture was designed to create a circular irradiation field with a $40\sqrt{2}$ cm diameter (the diagonal of a 40 x 40 cm^2 field) at 100 cm from the target;

d) The target and primary collimator were placed in a vacuum volume, where the primary electron beam is generated 5 mm upstream of the target; other structures are placed in air;
e) The vacuum-air interface is separated by a beryllium window;
f) Flattening filter: modeled using the G4Polycone solid (LT = 5 mm), resembling a stack of truncated cones;
g) Ionization chamber: consists of seven pairs of alternating Kapton® and copper layers interspersed with air gaps;
h) Mylar mirror: modeled with a specified tilt angle;
i) Secondary collimator: four rectangular tungsten blocks shaped to shield the X-ray beam for the maximum field size (LT = 50 mm).

The Varian HDMLC consists of 80 inner leaves (0.5 cm width at isocenter) and 40 outer leaves (1 cm). Each leaf is individually driven by a motorized screw through a slot. To account for beam divergence and minimize penumbra between adjacent leaves, the sides of the leaves are angled toward the source, and the leaf ends are rounded, maintaining relatively consistent penumbra across varying leaf positions [22].

2.2.3 Phase-space generation

Phase-space generation is divided into two stages. This dual-phase-space approach offers several advantages over using a single phase-space file such as:

- Improved Accuracy: By isolating the beam-shaping components, each phase-space file can be validated independently, reducing cumulative modeling errors.
- Reusability: PhSp01 can be reused across multiple treatment configurations, improving computational efficiency.

- Enhanced small-field fidelity: Separating the MLC modeling helps reduce statistical noise and geometric uncertainties, particularly important in stereotactic and IMRT simulations.

The first generates a PhSp after the Linac head components that most influence the beam (target, primary collimator, and flattening filter), and the second generates a PhSp after the patient-dependent components or beam modifiers (secondary collimator and/or MLC).

The detection volume for the first phase-space (PhSp01) was modeled as a cylinder with a 1 μm height along the Z-axis and a radius equal to the diagonal of the maximum field, positioned just below the flattening filter. The second phase-space (PhSp02) was modeled as a rectangular prism with the same height and X-Y dimensions corresponding to the field size, positioned immediately above or below the MLC. Phase space data were recorded every million detected particles. PhSp01 was saved in a custom text-based format (.qPhSp) developed for this work, while PhSp02 was saved in the IAEA-compliant format. The .qPhSp format includes a header (PhSp name, Z-position, XY extent) and particle data (position, direction, energy, statistical weight, particle type, and nStat). The PhSp02 writing method was based on the G4IAEAphspWriter class [19-21].

2.2.4 Data capture and simulation execution

For both PhSps, particle data are captured when they reach a sensitive volume defined by the G4SensitiveDetector class. The ProcessHits function extracts the position, direction, energy, type, and statistical weight, which are then passed to another class responsible for writing the data to file. At the beginning of each history, nStat is set to 1. When a particle reaches the sensitive volume, its information is saved and nStat is set to 0. For PhSp01, the uniform bremsstrahlung splitting variance reduction technique can be applied, where each bremsstrahlung photon is replicated N times, each with a statistical weight of 1/N. To begin PhSp simulation, the beam energy data collection was configured for 2 x 10^{13} events using the run.mac macro file. Beam data were initially collected using a 20 x 20 cm^2 open field as

specified in linac.mac. Subsequently, a field of 10 x 10 cm^2 was simulated to generate PhSp01 and PhSp02, by adjusting the field size and specifying either 1 or 2 to identify which PhSp to generate. Phase-space files were generated using 2 x 10^{13} primary histories, with statistical uncertainties below 1% in high-dose regions and computation times averaging 12 hours per simulation stage on an Ubuntu-based multicore system.

2.3. Measurements

Dosimetric measurements, including percentage depth doses and dose profiles, were conducted for the 6 MV photon beam from a Varian Trilogy linear accelerator at INCa I. A 10 cm x 10 cm field size was selected for these measurements to establish a reference baseline for comparison with smaller field sizes. The PTW PinPoint 3D chamber (model 31022), an ultra-small-volume ionization chamber with sensitive volume of 0.016 cm^3, was employed for high-precision dosimetry. This detector is specifically designed for high-energy phton beams and is well-suited for field sizes ranging from 2 x 2 cm^2 up to 40 x 40 cm^2, making it ideal for both conventional and small-field dosimetry applications. The chamber's compact size minimizes volume-averaging effects, ensuring accurate measurements even in steep dose gradient regions. A PTW Unidos E electrometer (model T10010) was used to record the ionization currents, providing high sensitivity and stability during measurements. The electrometer was calibrated according to standard protocols to ensure traceability to national standards. The experimental methodology, utilizing the water phantom at SSD = 100 cm, ensures reliable and reproducible data, forming the foundation for subsequent Monte Carlo simulations and small-field dosimetry corrections. The high precision of the PTW PinPoint 3D chamber, combined with the stability of the Unidos E electrometer, allows for detailed beam characterization, which is critical for advanced radiotherapy techniques such as stereotactic radiosurgery (SRS) and stereotactic body radiotherapy (SBRT).

The PTW PinPoint 3D chamber (model 31022) was selected due to its high spatial resolution, small sensitive volume (0.016 cm^3), and proven reliability in measuring photon

beams from 2x2 cm^2 up to 40×40 cm^2, making it well-suited for benchmarking intermediate small fields. Unlike diodes or microDiamond detectors, which are known for high sensitivity in very small fields (<1×1 cm^2), the PinPoint chamber minimizes volume-averaging effects while offering robust compatibility with conventional dosimetry systems. However, its performance is constrained for ultra-small fields (<1×1 cm^2), where steep dose gradients and lack of charged-particle equilibrium may lead to significant measurement uncertainty and signal perturbation. Ongoing work includes supplementary microdetector-based measurements to evaluate these extreme field sizes with improved accuracy.

3. RESULTS AND DISCUSSIONS

3.1. Monte Carlo simulations

The Monte Carlo (MC) simulations were conducted using the Geant4 framework on an Ubuntu platform to model a 6 MV Varian Trilogy Linac equipped with a high-definition multileaf collimator (HDMLC). The virtual models, designated as *qLinacs*, are illustrated in Figure 2. The accompanying mathematical phantom, *qMATphantom*, is a cubic water phantom (40 cm x 40 cm x 40 cm) designed for dose deposition studies.

Figure 2: Virtual models of the 6 MV Varian Linac (left) and the HDMLC (right).

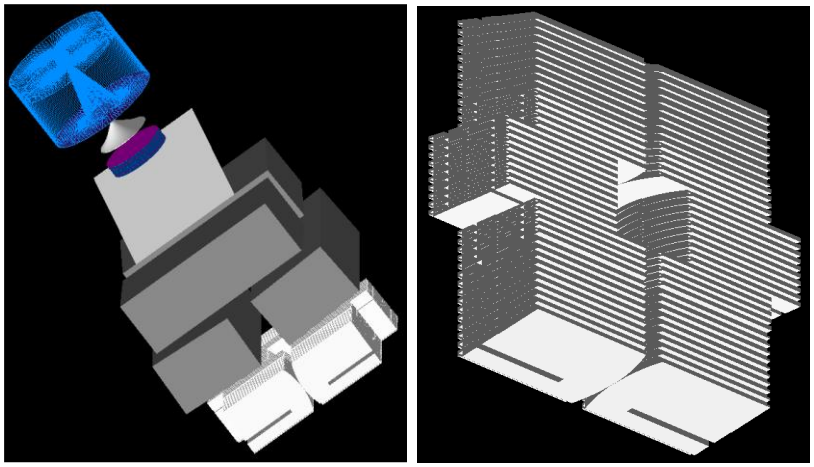

Source: The authors.

To ensure the accuracy of the Monte Carlo simulation pipeline, two complementary computational models were developed and validated: qMATphantom (a homogeneous water phantom for benchmarking dose deposition against established standards) and qLinacs (a Geant4-based model of the Varian Trilogy linear accelerator, including critical components like the target, primary collimator, flattening filter, and HDMLC). The qLinacs and qMATphantom models used in this study were originally developed and validated in previous works. The qLinacs model was validated as described by Holanda de Oliveira et al. (2018), who presented an experimental methodology for Monte Carlo modeling of multileaf collimators using the Geant4 code [23]. Meanwhile, the qMATphantom model is based on the Quimera platform, also developed by Holanda de Oliveira et al. (2018), designed for dose evaluation in radiotherapy through simulations with Geant4 [24]. These models are interdependent but serve distinct purposes: qMATphantom isolates dose calculation performance, while qLinacs ensures realistic beam generation and shaping. Dose calculations in qMATphantom utilized 10^9 particles sampled from the pre-generated phase-space files (PhSp01/PhSp02), which were originally simulated with 2×10^{13} primary events to ensure statistical reliability.

3.2. Phantom simulation and validation

The qMATphantom was validated against the EGSnrc-based *DOSXYZnrc* code using IAEA phase-space datasets [22-25]. Key validation metrics included percentage depth doses (PDDs) and lateral profiles, with tolerances of 1-2% in high-dose regions and < 20% in penumbral regions, as recommended by the IAEA TRS report 483 [9]. This step isolates the performance of the dose calculation engine (Geant4's physics models) from potential errors in the Linac geometry. The level of agreement is clinically significant, as it enables accurate output factor corrections in SRS, where small-field dosimetry is particularly sensitive. The qMATphantom's performance aligns with TG-155 and TRS-483 recommendations, supporting safer and more consistent dose delivery.

In Figure 3 is displayed the PPD's comparison between MC simulations and IAEA data for a 10 cm x 10 cm field. It is also shown the gamma index evaluation. The gamma index is a quantitative metric used in radiotherapy to compare two dose distributions - typically a calculated dose distribution (from a treatment planning system or Monte Carlo simulation) and a measured/reference dose distribution (from film, ionization chambers, or diode arrays) [26-34]. It evaluates both dose difference and spatial distance-to-agreement simultaneously, providing a unified measure of agreement. For each point in the evaluated dose distribution, the gamma index can be calculated as

Figure 3: Percentage depth dose (PDD) comparison between DOSXYZ (IAEA) and qMATphantom (MC) for a 10 x 10 cm² photon field (top), and the correspondent gamma index evaluation (bottom).

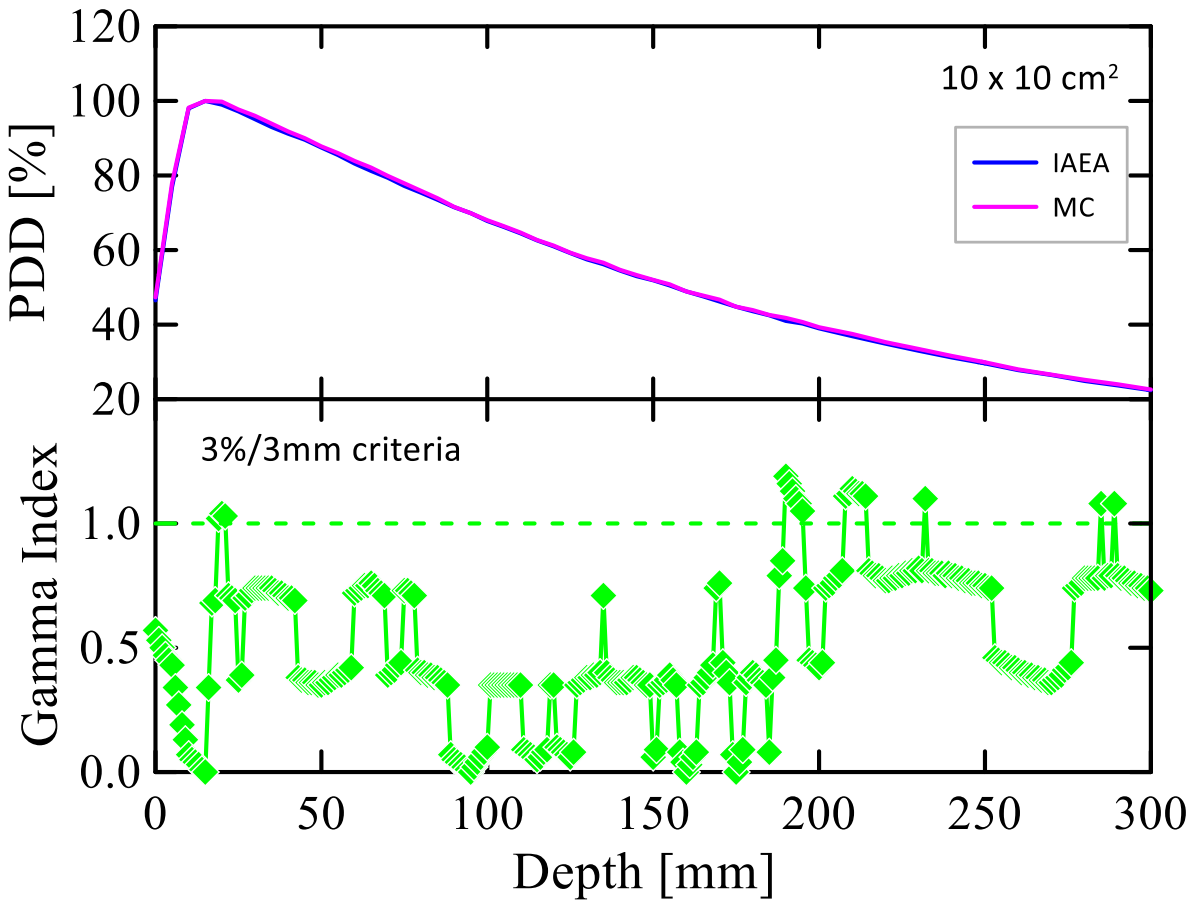

Source: The authors.

$$gamma\ index = \sqrt{\left(\frac{s}{DTA}\right)^2 + \left(\frac{d}{DD}\right)^2}, \quad (1)$$

where

- s = spatial distance between the evaluated dose and the closest dose in the reference distribution.
- d = dose difference between the evaluated and reference points.
- DTA = distance-to-agreement criterion (e.g., 3 mm).
- DD = maximum allowable dose difference (e.g., 3%).

A point passes if the gamma index ≤ 1 (i.e., the combined dose and spatial deviations are within tolerances).

The results shown in Figure 3 indicate that a significant portion of the dataset - more than 95% - successfully met the gamma analysis acceptance threshold based on the 3% dose difference and 3 mm distance-to-agreement (DTA) criteria. This high passing rate suggests a strong agreement between the evaluated dose distributions and the reference data. Furthermore, the analysis identified the largest observed dose deviation to be 1.95%, which occurred at a depth of 190 mm within the phantom. In terms of spatial agreement, the greatest deviation in the distance-to-agreement was measured as 3 mm, occurring at various depths. These findings highlight the overall accuracy of the dose calculation model, while also pinpointing the specific locations within the irradiated volume where the most significant discrepancies were detected. The gamma index evaluation was performed by using a Fortran code. While the gamma index provides a robust framework for comparing dose distributions, its sensitivity to noise and dependence on user-defined criteria introduce limitations. In this study, a 3%/3 mm criteria was selected in alignment with IAEA TRS-483 and AAPM TG-218 guidelines, ensuring consistency with clinical tolerances. However, applying stricter criteria (2%/2 mm) may reveal discrepancies in high-gradient regions,

particularly near field edges and buildup zones. Preliminary analysis showed a reduction in passing rates under 2%/2 mm, with gamma failures localized to penumbral areas and depths >200 mm-suggesting areas for refinement in beam modeling and MLC geometry.

Figure 4 depicts the lateral dose profiles of the percentage depth dose distribution evaluated at the depth corresponding to the maximum dose deposition (15 mm, typical for 6 MV photons). The comparison between the calculated and reference dose distributions was assessed using the percentage differences between the two dose distributions. The results revealed that 100% of the data points differ by less than 1% in the region of the photon field (-50 mm to 50 mm). Even in the penumbra regions the differences between the dose distributions remain < 1%, indicating a high level of concordance between the simulated and reference profiles. Additionally, it can also be observed that doses fall off to 80% of central value at the edge of the photon field; doses decrease to 60% at regions distant 55 mm from the center of the photon field, and doses are just 10% at 70 mm from the center of the field. These findings underscore the reliability of the dose calculation in reproducing the spatial dose distribution, particularly in the central photon beam region.

Figure 4: Top: Comparison of lateral percentage depth dose curves at 15 mm depth between DOSXYZ (IAEA) and qMATphantom (MC) for a 10 x 10 cm² photon field. Bottom: Differences between IAEA and MC doses.

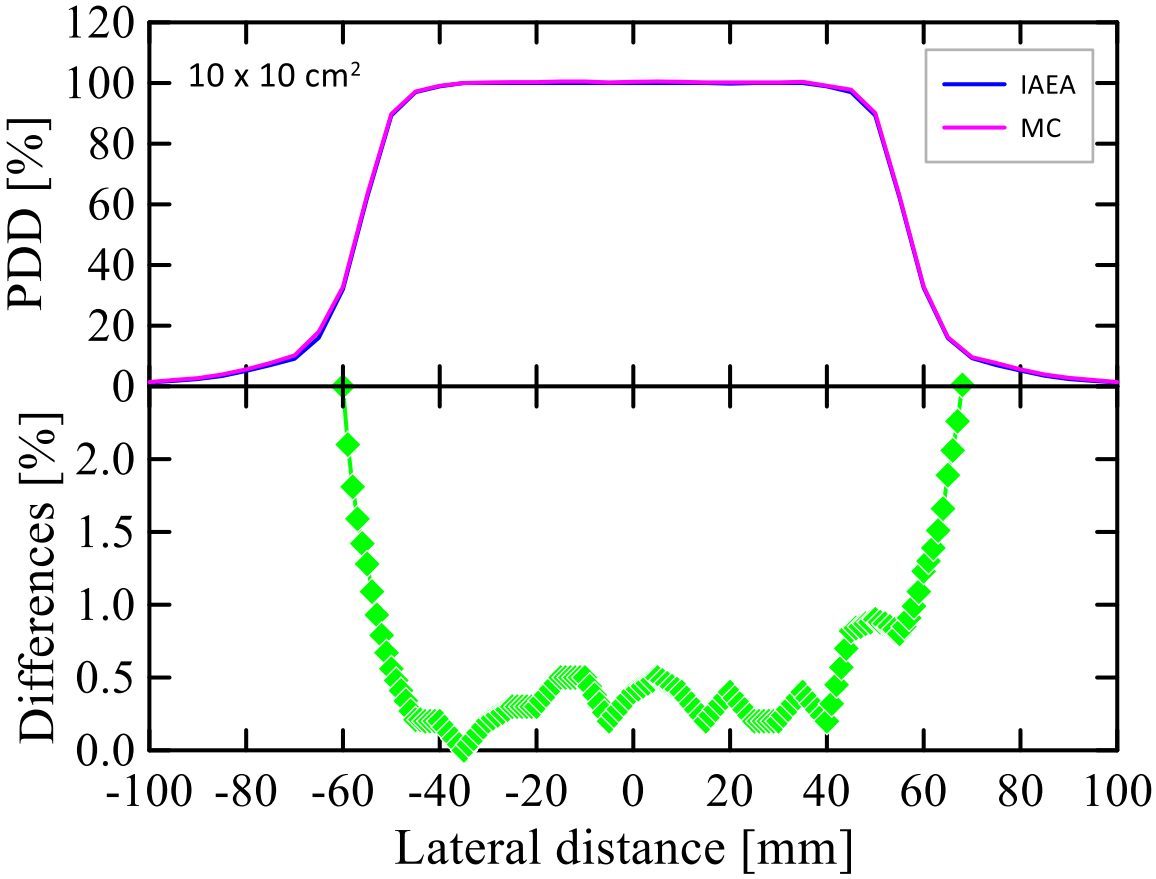

Source: The authors.

3.3. Linac simulation and validation

The qLinacs model replicates the physical components of the Varian Trilogy Linac, including the target, primary collimator, flattening filter, and high-definition multileaf collimator (HDMLC). Its primary purpose is to simulate the 6 MV photon beam and generate phase-space files (PhSp01 and PhSp02) at critical stages of beam modification (see section 2.2). Validation of qLinacs involved comparing simulated percentage depth dose curves and beam profiles against experimental measurements, and evaluating discrepancies in the penumbra region (attributed to MLC leaf modeling granularity) and high-dose regions

(mean error: ≤ 2%). This step ensures that the beam generation and shaping - including effects of collimators and MLC - are clinically realistic.

Figure 5 illustrates the percentage depth dose curves obtained from both Monte Carlo simulations and experimental measurements. A gamma index analysis was performed using the widely accepted 3% dose difference and 3 mm distance-to-agreement criteria to quantitatively assess the agreement between the two datasets. The results showed that more than 95% of the data points met these criteria, demonstrating a strong consistency between the simulated and measured dose distributions. Nevertheless, minor discrepancies were observed, with the largest dose difference reaching 2.6% at a depth of 0 mm and a maximum spatial deviation of 3 mm occurring at varying depths. These deviations can be attributed to several factors, including simplifications in the HDMLC leaf geometry and the resolution of the phase-space files used during simulation. Additionally, the Livermore electromagnetic physics model employed in Geant4 - while optimized for small-field dosimetry - may not fully capture all low-energy photon interactions or secondary electron transport effects. Measurement uncertainties may also contribute, especially in the build-up region, where the compact volume of the PinPoint 3D ionization chamber can result in volume averaging and positioning errors. Taken together, these results confirm the overall reliability of the MC simulation in reproducing the experimental PDD profile, while highlighting the complex interplay between modeling assumptions, physical processes, and detector limitations across build-up and high-gradient dose regions.

Figure 6 displays the lateral percentage depth dose distributions obtained from Monte Carlo (MC) simulations and experimental results, evaluated at the depth of maximum dose (15 mm). Percentage differences between simulated and measured doses were calculated. Results indicate that 95% of the data points differ by less than 1% in the region of the photon field (-50 mm to 50 mm), indicating a high level of concordance between the simulated and measured profiles. The largest differences occur at the edges of the photon field due to the

penumbra effect. However, in penumbra regions the dose differences remain within the acceptable clinical tolerance of 2% [33,34]. Notably, it can be observed that doses decline to 80% of central dose at the edge of the photon field; doses fall off to 60% at regions distant 55 mm from the center of the photon field, and doses diminish to 10% at 70 mm from the center of the field. In general, these results confirm the reliability of the MC model in accurately reproducing the lateral dose distribution at the depth of maximum dose.

Figure 5: Percentage depth dose (PDD) comparison between experimental (EXP) and qLinacs (MC) for a 10 cm x 10 cm photon field (top), and the correspondent gamma index evaluation (bottom).

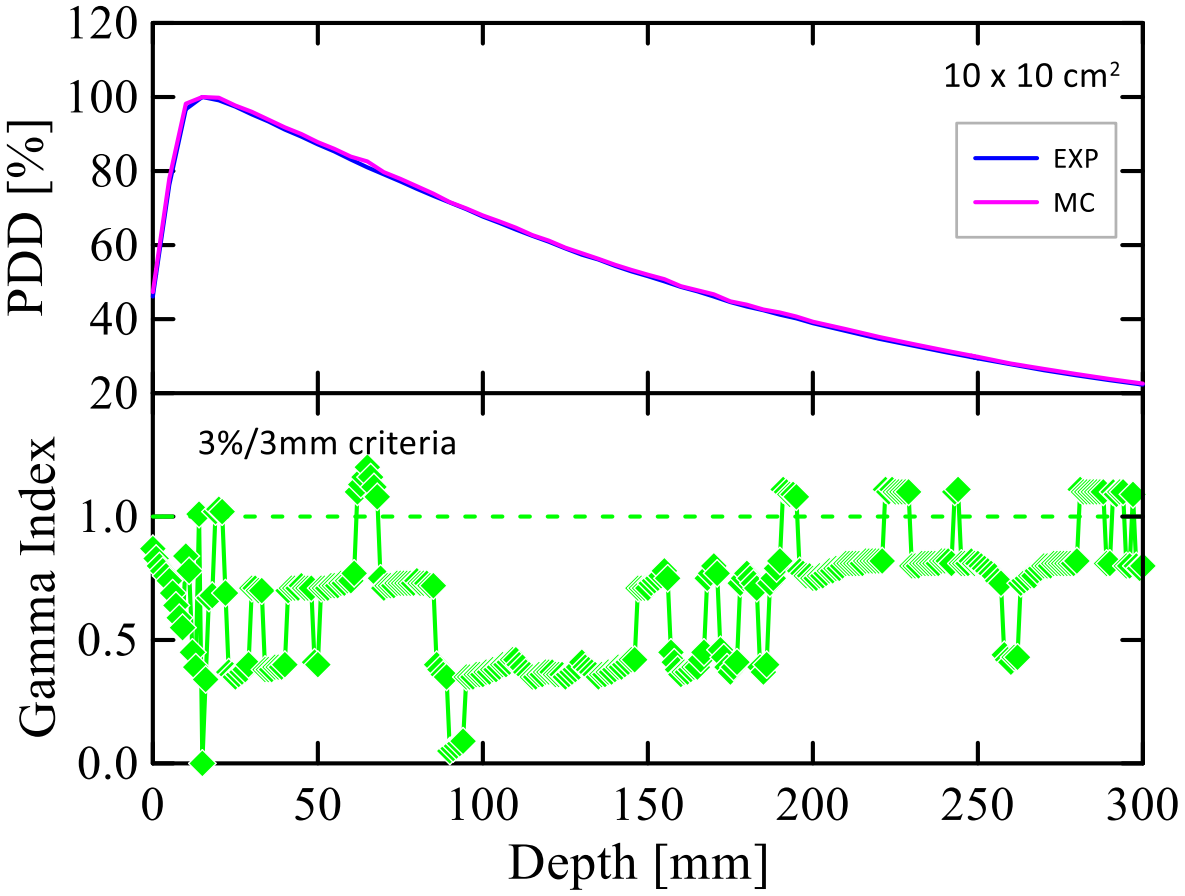

Source: The authors.

Figure 6: Top: Comparison of lateral percentage depth dose curves at 15 mm depth between experimental (EXP) and qLinacs (MC) for a 10 cm x 10 cm photon field. Bottom: Differences between EXP and MC doses.

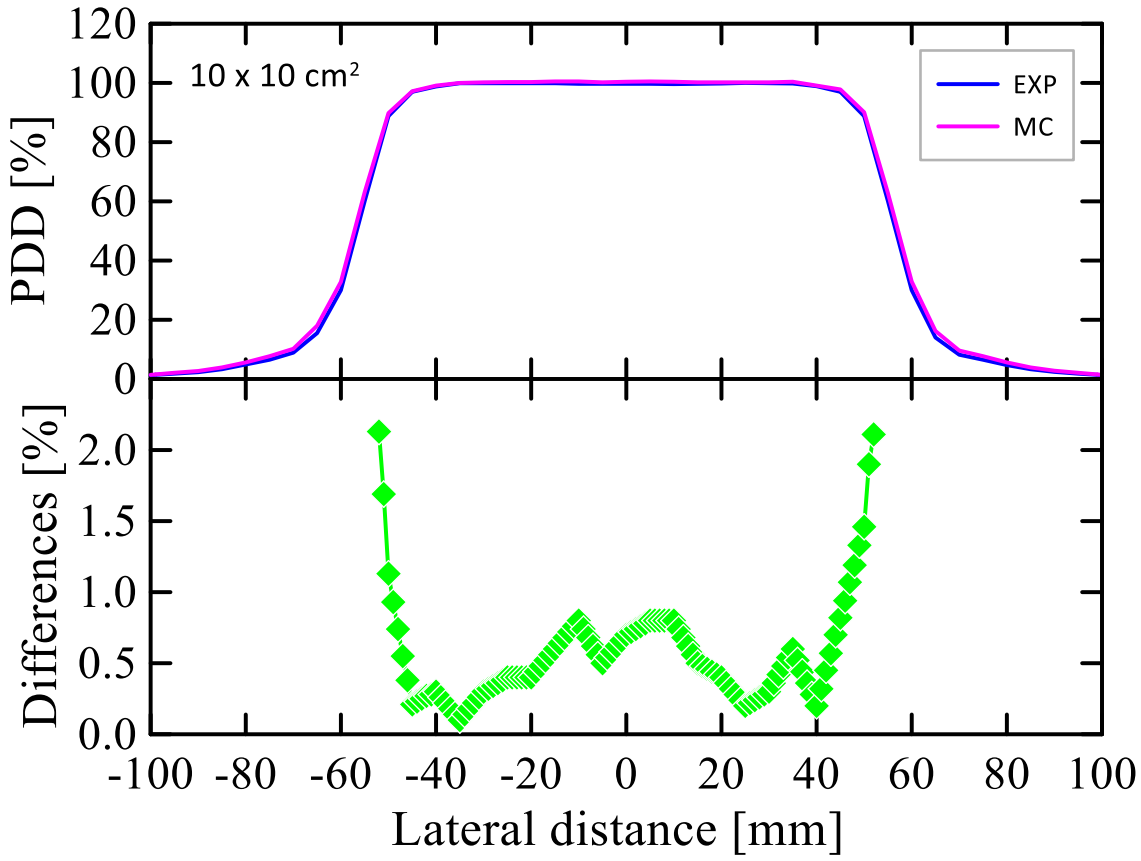

Source: The authors.

Although direct results for fields < 3 x 3 cm² are not included in this manuscript, subsequent phases of this research will address stereotactic cones and sub-centimeter MLC-defined fields. Future work will incorporate detector correction factors and expanded validation protocols, further strengthening the applicability of this modeling approach to highly modulated treatment scenarios.

4. CONCLUSIONS

The qLinacs and qMATphantom models demonstrated robust agreement with experimental and IAEA benchmarks, achieving dose agreement within <2% in high-dose regions and >95% gamma passing rates (3%/3 mm) for PDDs. To the best of our knowledge, this is the first Geant4-based implementation of a Varian Trilogy HDMLC model with experimental validation focused on small-field dosimetry. By independently validating dose calculation (qMATphantom) and beam generation (qLinacs), the framework provides a modular platform for extending MC simulations to other Linac models or complex geometries in SBRT/SRS applications.

Future developments will focus on refining MLC leaf modeling in qLinacs to reduce penumbral uncertainties. Small fields (<10 x 10 cm^2) exhibit significant output factor discrepancies due to volume averaging and lack of charged particle equilibrium. Detector-specific correction factors will be derived using MC simulations, guided by methodologies from IAEA TRS report 483. This is particularly critical for fields <3 x 3 cm^2, where uncorrected errors can exceed 5% based on published data. Penumbral modeling will be improved by incorporating rounded leaf-end effects in the HDMLC geometry. Furthermore, the framework will be extended to stereotactic cones (5-15 mm) and heterogeneous phantoms, leveraging existing small-field validation protocols.

In summary, this work establishes a reproducible pipeline for MC-based linac modeling, directly addressing the challenges of small-field dosimetry in advanced techniques such as SBRT, IMRT, and VMAT.

ACKNOWLEDGMENT

The authors would like to thank the Instituto de Radioproteção e Dosimetria and the Instituto Nacional de Cancer for their support.

CONFLICT OF INTEREST

The authors declare that they have no conflicts of interest.

REFERENCES

[1] CHETTY, I. J.; MARTEL, M. K.; JAFFRAY, D. A.; BENEDICT, S. H.; HAHN, S. M.; BERBECO, R.; DEYE, J.; JERAJ, R.; KAVANAGH, B.; KRISHNAN, S.; LEE, N.; LOW, D. A.; MANKOFF, D.; MARKS, L. B.; OLLENDORF, D.; PAGANETTI, H.; ROSS, B.; SIOCHI, R. A.; TIMMERMAN, R. D,; WONG, J. W. Technology for innovation in radiation oncology. **International Journal of Radiation Oncology. Biology. Physics**, v. 93, n. 3, p. 485-492, 2015.

[2] BAUMANN, M.; KRAUSE, M.; OVERGAARD, J.; DEBUS, J.; BENTZEN, S. M.; DAARTZ, J.; RICHTER, C.; ZIPS, D.; BORTFELD, T. Radiation oncology in the era of precision medicine. **Nature Reviews Cancer**, v. 16, n. 4, p. 234-249, 2016.

[3] KOKA, K.; VERMA, A.; DWARAKANATH, B. S.; PAPINENI, R. V. L. Technological advancements in external beam radiation therapy (EBRT): An indispensable tool for cancer treatment. **Cancer Management and Research**, v. 14, p. 1421-1429, 2022.

[4] WAHABI, J. M.; WONG, J. H. D.; MAHDIRAJI, G. A.; UNG, N. M. Feasibility of determining external beam radiotherapy dose using LuSy dosimeter. **Journal of Applied Clinical Medical Physics**, v. 25, n. 6, p. e14387, 2024.

[5] KINOSHITA, N.; SHIMIZU, M.; MOTEGI, K.; TSURUTA, Y.; TAKAKURA, T.; OGUCHI, H.; KUROKAWA, C. Quantification of uncertainties in reference and relative dose measurements, dose calculations, and patient setup in modern external beam radiotherapy. **Radiological Physics and Technology**, v. 18, n. 1, p. 58-77, 2024.

[6] DUAN, W.; WU, H.; ZHU, Y.; ZHAO, G.; ZHANG, C.; JIANG, J.; FAN, Z.; WANG, Z.; WANG, R. Dosimetric comparison of gamma knife and linear accelerator (VMAT and IMRT) plans of SBRT of Lung tumours. **Scientific Reports**, v. 14, n. 1, p. 22949, 2024.

[7] YANI, S. ; RHANI, M. F. ; SOH, R. C. X.; HARYANTO, F. ; ARIF, I. Monte Carlo simulation of varian clinac iX 10 MV photon beam for small field dosimetry. **Internation Journal of Radiation Research**, v. 15, n. 3, p. 275-282, 2017.

[8] BAGHERI, H.; SOLEIMANI, A.; GHAREHAGHAJI, N.; MESBAHI, A.; MANOUCHEHRI, F.; SHEKARCHI, B.; DORMANESH, B.; DADGAR, H. A. An overview on small-field dosimetry in photon beam radiotherapy: Developments and challenges. **Journal Cancer Research and Therapeutics**, v. 13, n. 2, p. 175-185, 2017.

[9] IAEA TRS report 483. Dosimetry of small static fields used in external beam radiotherapy. INTERNATIONAL ATOMIC ENERGY AGENCY, Vienna 2017.

[10] PALMANS, H.; ANDREO, P. HUQ, M. S.; SEUNTJENS, J.; CHRISTAKI, K. E.; MEGHZIFENE, A. Dosimetry of small static fields used in external photon beam radiotherapy: Summary of TRS-483, the IAEA-AAPM international Code of Practice for reference and relative dose determination. **Medical Physics**, v. 45, n. 11, p. e1123-e1145, 2018.

[11] GHOLAMI, S. ; LONGO, F. ; NEDAIE, H. A. ; BERTI, A. ; MOUSAVI, M.; MEIGOONI, A. S. Application of Geant4 Monte Carlo simulation in dose calculations for small radiosurgical fields, **Medical Dosimetry**, v. 43, n. 3, p. 214-223, 2018.

[12] CHI, D. D.; TOAN, T. N.; HILL, R. A multi-detector comparison to determine convergence of measured relative output factors for small field dosimetry. **Physical and Engineering Sciences in Medicine**, v. 47, n. 1, p. 371-379, 2024.

[13] SPENKELINK, G. B.; HUIJSKENS, S. C.; ZINDLER, J. D.; DE GOEDE, M.; VAN DER STAR, W. J. VAN EGMOND, J.; PETOUKHOVA, A. L. Comparative assessment and QA measurement array validation of Monte Carlo and Collapsed Cone dose algorithms for small fields and clinical treatment plans. **Journal of Applied Clinical Medical Physics**, v. 25, n. 12, p. e14522, 2024.

[14] ANDREO, P. Monte Carlo simulations in radiotherapy dosimetry. **Radiation Oncology**, v. 13, n. 1, p. 121, 2018.

[15] OHIRA, S.; TAKEGAWA, H.; MIYAZAK, M.; KOIZUMI, M.; TESHIMA, T. Monte Carlo modeling of the Agility MLC for IMRT and VMAT calculations. **In Vivo**, v. 34, p. 2371-2380, 2020.

[16] ZHANG, F.; ZHOU, M.; LIU, J.; YUE, L.; DENG, L.; XU, Z; WANG, G. Benchmarking of electron beam parameters based on Monte Carlo linear accelerator simulation. **Translational Cancer Research**, Hong Kong, v. 9, n. 2, p. 577-584, 2020.

[17] RENIL MON, P. S.; MEENA-DEVI, V. N.; BHASI, S. Monte Carlo modelling and validation of the elekta synergy medical linear accelerator equipped with radiosurgical cones. **Heliyon**, v. 9, n. 4, p. e15328, 2023.

[18] Varian Medical System. Available in: https://www.varian.com/en-au/products/radiotherapy/treatment-delivery/trilogy. Accessed in: November 5, 2024.

[19] Geant4 Collaboration. International Geant4 Collaboration. Available in: https://geant4.web.cern.ch/collaboration/. Accessed in: January 26, 2025.

[20] Book For Application Developers. Available in: https://geant4-userdoc.web.cern.ch/UsersGuides/ForApplicationDeveloper/html/index.html. Accessed in: Dezember 5, 2024.

[21] MyVarian. Available from: https://www.myvarian.com/. Accessed in: January 26, 2025.

[22] HEATH, E.; SEUNTJENS, J. Development and validation of a BEAMnrc component module for accurate Monte Carlo modelling of the Varian dynamic Millennium multileaf collimator. **Physics in Medicine and Biology**, v. 48, n. 24, p. 4045, 2003.

[23] HOLANDA DE OLIVEIRA, A. C.; VIEIRA, J. W.; ZARZA MORENO, M.; ANDRADE LIMA, F. R. Experimental verification of a methodology for Monte Carlo modeling of multileaf collimators using the code Geant4. **Brazilian Journal of Radiation Sciences**, v. 6, n. 2, p. 1-14, 2018.

[24] HOLANDA DE OLIVEIRA, A. C.; VIEIRA, J. W.; LIMA, F. R. A. Quimera: a simulation platform based on the code Geant4 for dose evaluation in radiotherapy. **Brazilian Journal of Radiation Sciences**, v. 6, n. 3, p. 1-18, 2018.

[25] AAPM Report n. 72. Basic Applications of multileaf collimators. AMERICAN ASSOCIATION OF PHYSICISTS IN MEDICINE, Madison 2001.

[26] CORTÉS-GIRALDO, M. A.; QUESADA, J. M.; GALLARDO, M. I.; CAPOTE, R. An implementation to read and write IAEA phase-space files in GEANT4-based simulations. **International Journal of Radiation Biology**, v. 88, n. 1-2, p. 200-208, 2012.

[27] LOW, D. A.; HARMS, W. B.; MUTIC, S.; PURDY, J. A. A technique for the quantitative evaluation of dose distributions. **Medical Physics**, v. 25, n. 5, p. 656-661, 1998.

[28] LOW, D. A.; DEMPSEY, J. F. Evaluation of the gamma dose distribution comparison method. **Medical Physics**, v. 30, n. 9, p. 2455-2464, 2003.

[29] CHEN, M. ; LU, W. ; CHEN, Q. ; RUCHALA, K. ; OLIVEIRA, G. Efficient gamma index calculation using fast Euclidean distance transform. **Physics in Medicine and Biology**, v. 54, p. 2037-2047, 2009.

[30] HENG LI, H.; DONG, L.; ZHANG, L.; YANG, J. N.; GILLIN, M. T.; ZHU, X. R. Toward a better understanding of the gamma index: Investigation of parameters with a surface-based distance method. **Medical Physics**, v. 18, n. 12, p. 6730-6741, 2011.

[31] HUSSEIN, M.; CLARK, C. H.; NISBET, A. Challenges in calculation of the gamma index in radiotherapy - Towards good practice. **Physica Medica**, v. 36, p. 1-11, 2017.

[32] DAS, S.; KHARADE, V.; PANDEY, V.; ANJU, K. V.; PASRICHA, R. K.; GUPTA, M. Gamma index analysis as a patient-specific quality assurance tool for high-precision radiotherapy: A clinical perspective of single institute experience, **Cureus**, v. 14, n. 10, p. e30885, 2022.

[33] TAI, D. T.; OMER, H.; QUOC, L. C.; HAI, N. X.; MINH, T. V.; SULIEMAN, A.; MATTAR, E.; TOUFIG, H.; TAMAM, N.; BRADLEY, D. A. An open-source software for calculating 1D gamma index in radiation therapy. **Journal of King Saud University - Science**, v. 35, n. 10, p. 102937, 2023.

[34] ICRU report 24. Determination of absorbed dose in a patient irradiated by beams of X or gamma rays in radiotherapy. INTERNATIONAL COMMISSION ON RADIATION UNITS AND MEASUREMENTS, Bethesda 1976.

[35] MIFTEN, M.; OLCH, A.; MIHAILIDIS, D.; MORAN, J.; PAWLICKI, T.; MOLINEU, A.; LI, H.; WIJESOORIYA, K.; SHI, J.; XIA, P.; PAPANIKOLAOU, N; LOW, D. A. Tolerance limits and methodologies for IMRT measurement-based verification QA: Recommendations of AAPM Task Group No. 218. **Medical Physics**, v. 45, p. e53-e83, 2018.

LICENSE